Applied Acoustics 231 (2025) 110559

Contents lists available at ScienceDirect

Applied Acoustics

journal homepage: www.elsevier.com/locate/apacoust

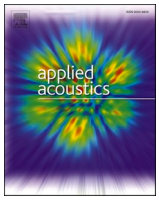

Infrasound produced by a small pile fire

J.B. Johnson [a,*], J.F. Anderson [a], K. Yedinak [b]

[a] Department of Geosciences, Boise State University, United States
[b] USDA Forest Service, Northern Research Station, United States

ARTICLE INFO

Keywords:
Infrasound
Array processing
Wildfire monitoring
Natural hazards

ABSTRACT

We document the characteristics of infrasound from a compact (<3-m burn diameter) wood pile fire using arrays located at 50 and 600 m. Infrasound from our controlled burn is present throughout the entire near-infrasound range (1–20 Hz), but its peak infrasound energy trends from 1.3 to 1 Hz over an hour correlating with a transition from relatively tall and narrow flame to a broader pile of coals with shorter flame. Observed infrasound frequencies correlate with flame flickering – quantified through spectral analysis of video – suggesting that flame and gas pulsing is the mechanism for the <2 Hz infrasound. Although the amplitude of the pile fire infrasound is low (<0.1 Pa at 50 m) it is a stationary source and detectable using array processing at 600 m. Given this demonstrated capability for remote surveillance of a small fire we contend that remote infrasound monitoring has potential application for larger wildfires.

1. Introduction

Infrasound is a widely used monitoring tool for hazardous processes occurring at Earth's surface and in the atmosphere, including volcanoes [1], anthropogenic explosions [2], mudflows [3], bolides [4], whitewater [5], tornadoes [6], earthquakes [7], and eruptions [8]. Hazard monitoring applications for infrasound largely fall into two categories. First, infrasound serves to detect hazardous activity and describe it quantitatively (for example, estimating the volume of gas erupted from a volcano or the yield of an explosion) and qualitatively (for example, identifying the style of eruptive activity as explosive, jetting, or repeated bursts) (e.g., [1]). Second, infrasound provides information on processes with uncertain locations (e.g., distinguishing between volcanic vents, or tracking fast-moving mudflows) by comparing infrasound travel times to multiple sensors belonging to a network and/or in an array, which can be used to determine the direction to the source (e.g., [9,10]).

Despite its demonstrated potential for research and real-time monitoring of other hazards, and the recognition that climate change will increase the frequency, severity, and size of wildfires [11], infrasound monitoring of wildland fire remains little-explored. Large fires from wood structures and storage facilities have been observed to produce infrasound that has been detected at least as far as 12 km away [12]. And more recently, infrasound has been reported for wildland fires, including prescribed fires in both forests and rangeland (e.g., [13,14]). Infrasound array analysis has succeeded in tracking wildland fire spread in a relatively low-intensity range fire [14] despite the presence of aircraft noise and little shielding from wind noise; its success in these difficult conditions indicates that the method could perform well near hazardous wildfires where more intense infrasound generation is expected.

The proposed mechanism for infrasound generation from diffuse flame sources is an instability whereby the fire periodically creates unstable buoyant plumes, referred to as "puffing" [15]. In fires burning over pools of liquid fuel (pool fires), a proportionality has been found between the square root of flame diameter and puffing frequency [16]; however, this relationship remains untested in wood fires (either in structures or wildlands). By contrast, audible and ultrasound emissions from fire are produced by different processes including turbulence along the fire-air boundary [17] and rupturing of plant tissues in fuel [18]. In this paper, we examine fire infrasound source processes from a small pile fire, showing correspondence between infrasound frequencies and periodic thermal signals in video observation. Further, we demonstrate that even small meter-scale fires can produce infrasound between 1 and 20 Hz that can be detected at a range of more than half a kilometer.

2. Experiment and data

The focus of this study was to record sounds associated with a compact-source controlled outdoor fire (referred to here as a pile fire) that was ignited near Stanley Idaho (USA) on January 14th, 2024. The

* Corresponding author at: 1910 University Drive, Boise, ID 83725, United States.
E-mail address: jeffreybjohnson@boisestate.edu (J.B. Johnson).

https://doi.org/10.1016/j.apacoust.2025.110559
Received 16 October 2024; Received in revised form 7 January 2025; Accepted 24 January 2025
Available online 28 January 2025

experiment consisted of a 2-m-high, ~3-m-diameter pyramidal pile of dry lodgepole pine (Pinus contorta) and Douglas-fir (Pseudotsuga menziesii), whose timber (ranging from 10 to 23 cm diameter) was dry and had been collected prior to seasonal snowfall. Our fire was ignited at 4:50 PM local time (23:50 UTC), grew rapidly in size until 4:53 (23:53 UTC), and had reduced to hot coals, with no significant flame, by 9:45 PM (04:45 UTC). During the first few hours of the experiment logs were sporadically added to the pile fire. Conditions during the experiment were cold (~−10 °C) and windless, providing for a low-noise infrasound recording environment. Conditions in the month prior to the experiment had been continuously below freezing and mostly dry. A ~1 m thick powdery snowpack was present in the area of the fire on the day of the experiment.

We recorded the pile fire with two 3-element infrasonic microphone arrays, a video camera recording at 25 frames per second (fps), and a timelapse camera with variable frame rate averaging 1 fps. The continuous microphone acquisition at 400 Hz was chosen to sample both infrasound (less than 20 Hz) as well as potential audible-band fire sounds up to a Nyquist frequency of 200 Hz. The two microphone arrays consisted of identical infraBSU version 2 infrasound sensors with flat response above ~0.1 Hz. Infrasound arrays are a common tool for detecting signal and identifying backazimuth to sources. They consist of multiple microphones positioned at ground level and separated from a station center (Fig. 1a). In the case of this experiment we spread 15-m cables like spokes from the station center and surveyed the relative positions of all sensors using a GPS Geode GNSS receiver at FB (accurate to within 1 m) and a compass and measuring tape at FA (Fig. 1b). The array centers for FA and FB were 50 m East and 600 m North of the fire respectively. Data were recorded continuously with a DiGOS DataCube 24-bit, 3-channel datalogger with GPS time synchronization. The infraBSU sensors were operationally similar to those described in [19] and [20].

Because most of the coherent signal recorded by the microphone arrays was below 20 Hz we refer to the collected data as infrasound. Fig. 2 shows 3.5 h of data recorded with both arrays filtered to select bands. At FA the infrasound is first evident starting at 16:50, when the pile is initially ignited, and increased in amplitude until 16:53 as the intensity of the pile fire and its flame height grew larger. No bonfire infrasound is visually evident on the FB waveforms (at 600 m), but array FA (at 50 m) displays identifiable tremor that is relatively stationary in the 1–5 Hz, 5–10 Hz, 10–20 Hz, and 20 Hz-40 Hz bands beginning with the pile fire's inception (at 4:50 PM local time) and lasting until at least 6:00 PM. The high-amplitude tremor in the 0.1 to 1 Hz band is equally evident on both arrays, but this signal is remote microbarom infrasound (e.g., [21]) originating from relatively high elevation angles and from a generally southwest backazimuth. Additional higher-frequency short-duration signal transients, evident on both arrays occurring at 5:19, 5:35, 5:53 PM, 7:11 PM, and 7:34 PM, are attributed to air traffic. Other very short-duration pulses are evident only at array FA (e.g., at 6:27 to 6:30 PM) and correspond to a nearby parked car's door opening and closing. Finally, a drone was flown over the fire intermittently during the experiment and although it produced audio noise it could not be observed in the infrasonic bands.

Infrasound signal is correlated with video from both the (~1 fps) timelapse and continuous video (25 fps) using two Atli Eon cameras situated ~20 m from the pile fire. Field of view of the cameras indicated in Fig. 1b is 72°. These cameras, including an audio channel from the continuous video, were used to qualitatively estimate the size of the pile fire over time using color thresholding. Of note, camera automatic exposure adjustment occurred as day transitioned to night (i.e., sunset at 5:25 PM and civil twilight at 5:57 PM) and this inhibited quantitative analysis of flame brightness.

Fig. 3 relates the video-derived flame height to infrasound spectrograms and signal detection. Flame height chronology is calculated from a cropped 200 × 500 pixel window (annotation shown in Fig. 1c and d) and averaged over 30 s time intervals. Flame height information is

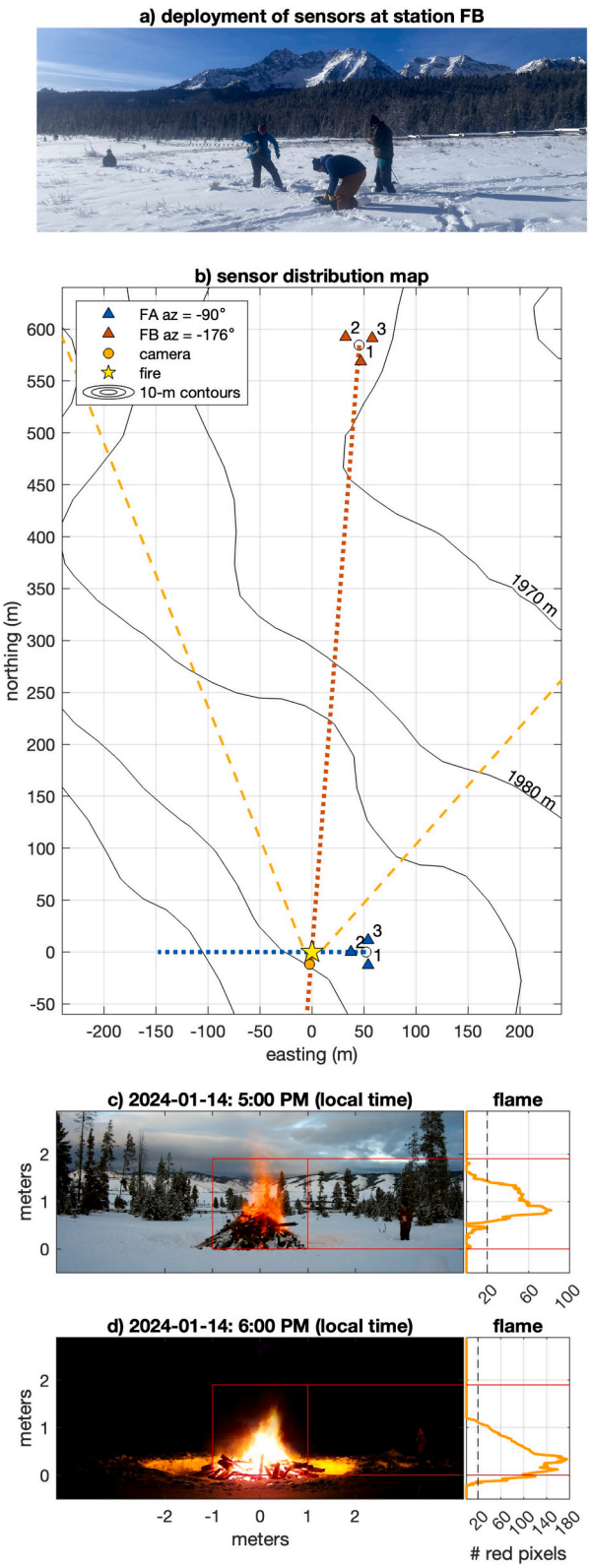

Fig. 1. Infrasound array deployment. (a) Photo showing deployment of infrasonic microphones at station FB (600 m from fire). (b) Map shows 3-element arrays for station FA, FB, and camera site with field of view indicated by dashed yellow lines. Photos from (c) 5 PM and (d) 6 PM have vertical and horizontal scales appropriate for fire. Profiles at right show the number of red pixels as a function of height; they are used as a flame height proxy shown in the time series in Fig. 3a.

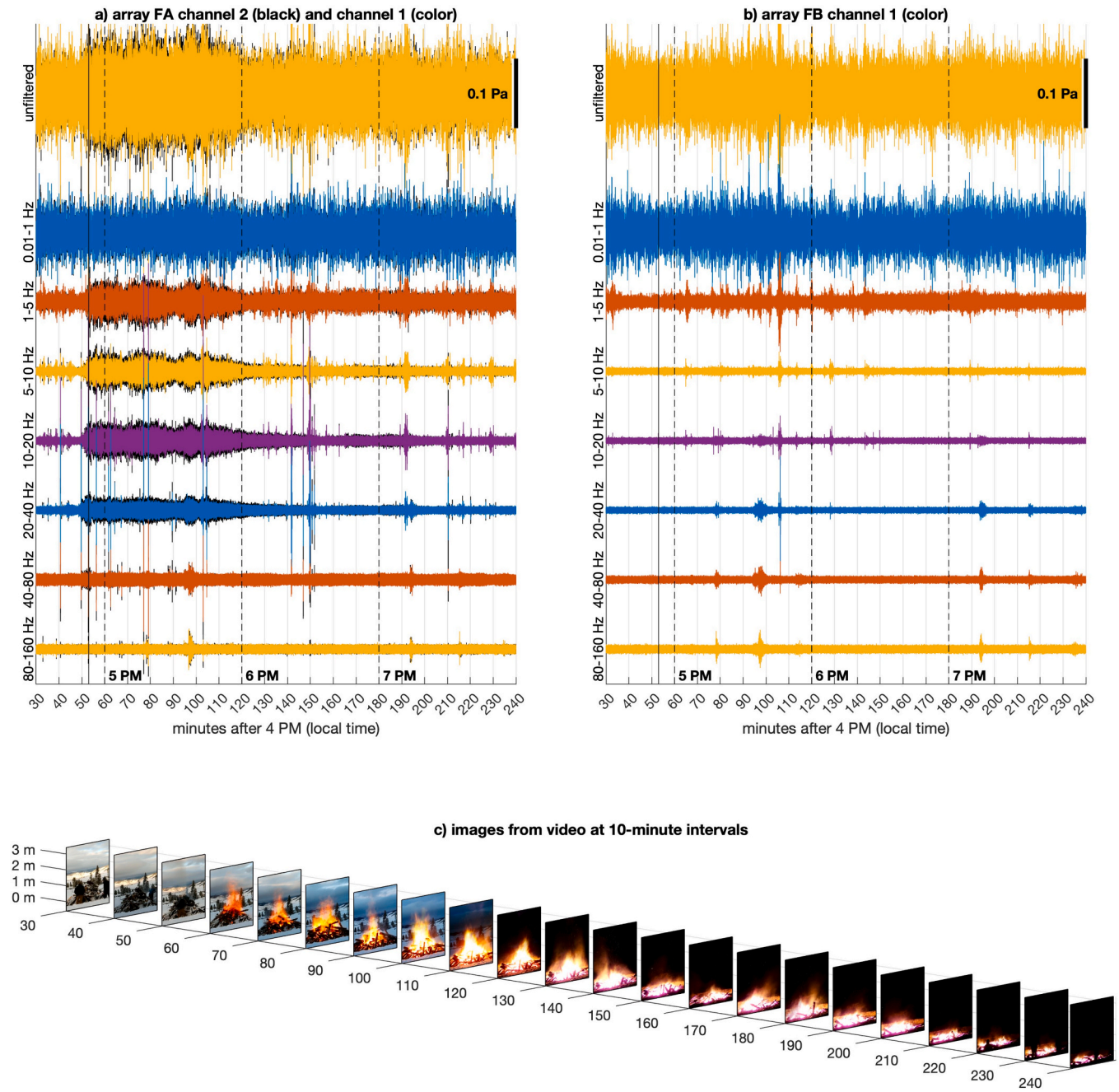

Fig. 2. 3.5 h waveforms and corresponding time-synchronized video image stills. (a and b) Infrasound from stations FA and FB have been filtered into indicated bands using two-pole bandpass filters. c) Still images are extracted from video at 10-min intervals.

extracted at each time step using only the red color band where each video frame is converted to a binary image with a value of 1 assigned to color values above 225 counts (out of 256 color levels). The number of *bright* pixels is then summed as a column vector and plotted as a function of time in Fig. 3a. The same processing applied to a horizontal summation gives a qualitative sense for the pile fire's width (Fig. 3b).

3. Methods

3.1. Array processing

Although pile fire infrasound is not visually evident in the infrasonic waveforms recorded at 600 m (e.g., Fig. 2b), it is identifiable at this distant array through cross-correlation analysis in the 5–15 Hz filter band (e.g., Fig. 3d). Comparison of infrasound from two sensors within an array is used to identify frequency bands of coherence. In Fig. 3 successive 30-second windows are analyzed and their normalized cross-correlation function $\boldsymbol{r}(\boldsymbol{\delta\tau}, \boldsymbol{t})$ is calculated as a function of lag time ($\boldsymbol{\delta\tau}$) and chronological time ($\boldsymbol{t}$). For array FA the correlation analysis is shown for a 0.3 to 20 Hz pass band because the pile fire signal is broadband. More than an hour of fire signal is evident at FA with a lag time of $\boldsymbol{\delta\tau}_{21} = -0.06$ s for channels 2 and 1. At array FB, coherence for the fire source is identifiable between 5 and 15 Hz with a fire-sourced lag time $\boldsymbol{\delta\tau}_{21} = +0.07$ s. At station FB (600 m) it appears as though infrasonic frequencies below 5 Hz are obscured by other sources of infrasound or noise. Persistent non-fire noise sources, including microbaroms and possible cultural infrasound from a metropolitan area ~150 km to the WSW, are evident both prior to fire onset and after the pile fire has

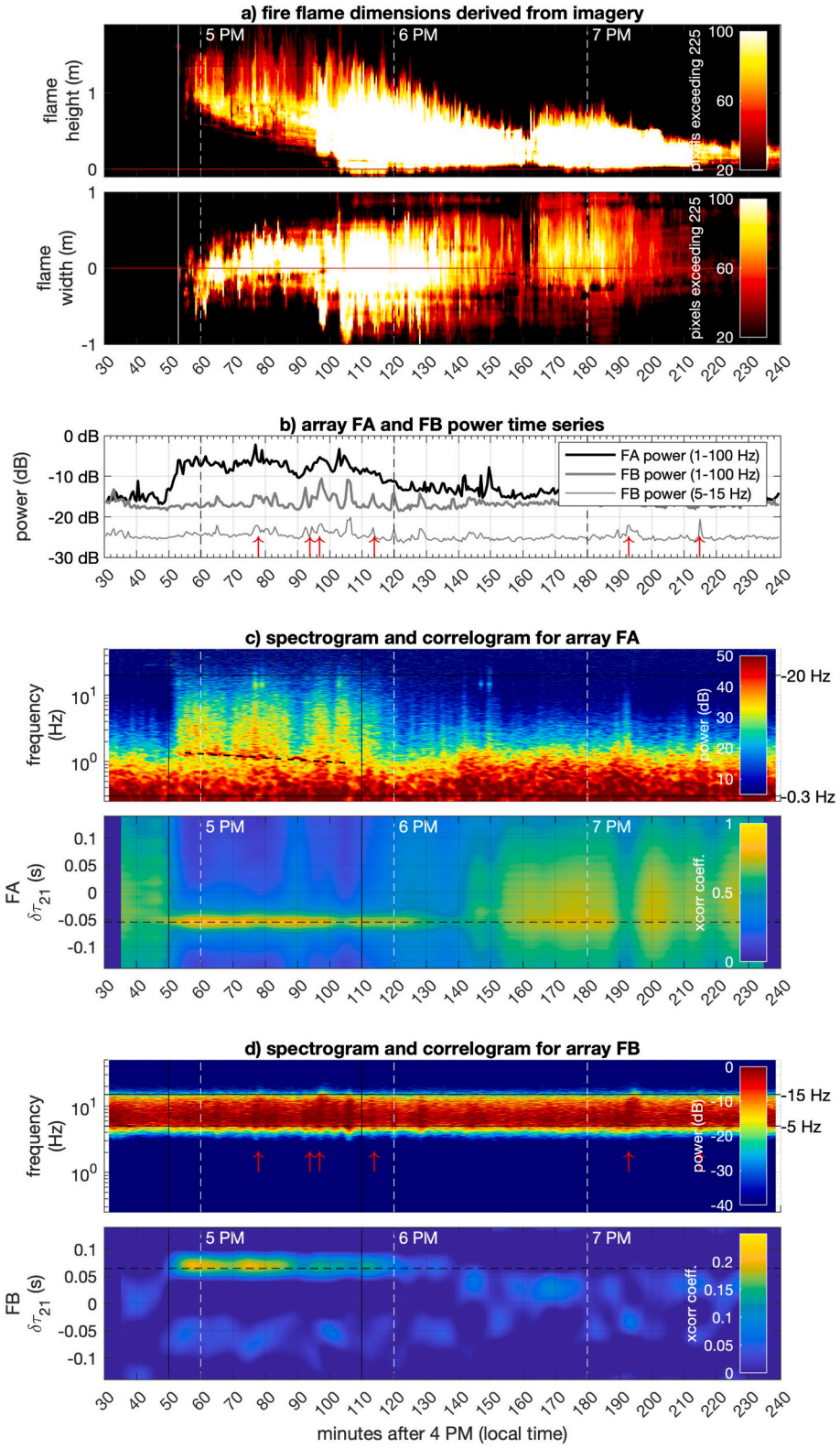

Fig. 3. Fire size chronology compared with infrasound spectral characteristics and signal correlation. (a) Time series flame height and width proxies are extracted from video at 30 s intervals. (b) Infrasound array power is calculated for array FA using the 1–100 Hz band and both the 1–100 Hz band and the 5–15 Hz band for array FB. Top panels of (c) and (d) show spectrograms for FA and FB for data filtered in the 0.3–100 Hz and 5–15 Hz bands respectively. Black dashed line in the spectrogram in (c) shows a spectral trend for which details are provided in Fig. 5. Bottom panels of (c) and (d) show running cross correlation analysis between channels 1 and 2 and respective frequency bands 0.3–20 Hz and 5–15 Hz for FA and FB. Expected time lags for fire-sourced infrasound are indicated with black dashed horizontal lines. Aircraft detections are indicated with vertical red arrows.

burned down.

Array processing using three channels of data and select filter bands is used to identify signal backazimuths. Signal correlation analyses in Fig. 4 are calculated as a grid search for all possible back azimuths (θ) and elevation angles ($\boldsymbol{\phi}$). For a single pair of infrasound channels (a compared with b) the normalized cross correlation function $\boldsymbol{r}(\theta, \boldsymbol{\phi}, \boldsymbol{t})$ is calculated using channel positional information (for b and a) and an assumed sound speed of $c = 325$ m/s. The product of three independent correlation functions are then used to identify incident source(s), e.g. for a three-element array:

$$\boldsymbol{S}(\theta, \boldsymbol{\phi}, \boldsymbol{t}) = \boldsymbol{r}_{21}(\theta, \boldsymbol{\phi}, \boldsymbol{t}) \bullet \boldsymbol{r}_{32}(\theta, \boldsymbol{\phi}, \boldsymbol{t}) \bullet \boldsymbol{r}_{13}(\theta, \boldsymbol{\phi}, \boldsymbol{t})$$

where $\boldsymbol{r}_{21}$, $\boldsymbol{r}_{32}$, and $\boldsymbol{r}_{13}$ are all greater than zero. High values of $\boldsymbol{S}$, analogous to semblance [22], indicate consistent, correlated signal from

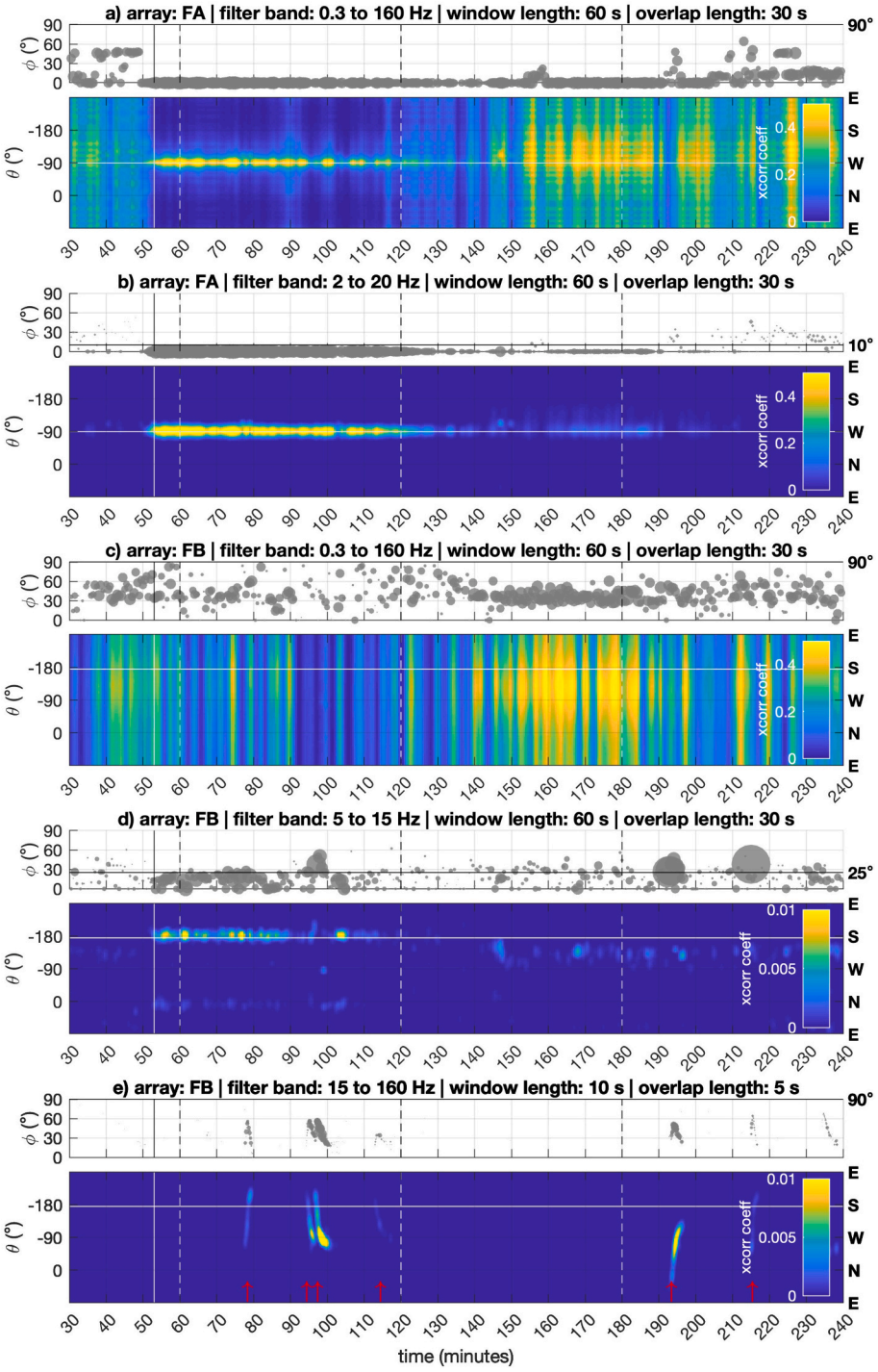

Fig. 4. Backazimuth (θ) and elevation angle (ϕ) of incident infrasound for both arrays and for indicated frequency bands. Symbol size in elevation angle plots are scaled to the band-filtered infrasound cross spectrum power. Horizontal white lines indicate the backazimuth direction to fire from arrays FA (−90°) and FB (-180°) respectively. (a) Broad band filtered data for FA show both fire infrasound (after 50 min) and prevalent microbarom/cultural infrasound before and after primary pile burn activity. (b) Fire infrasound is particularly well identified at FA in the near-infrasound band 2–20 Hz. (c) The broadly filtered data for array FB do not reveal the fire source due to diminished signal with respect to noise, however the 5–15 Hz filter band in (d) is able to detect the fire at FB. (e) A high frequency band above 15 Hz is effective for detecting non-fire moving sources with high elevation angles associated with passing aircraft (red arrows).

which back azimuth and elevation angles can be identified. The width of the semblance function $\boldsymbol{S}(\boldsymbol{t})$ provides a sense of azimuthal uncertainty. Notably backazimuth precision is greater for high frequency signals (e.g., Fig. 4e) where infrasound wavelength is short relative to array dimensions. Fig. 4 shows that dominant sources of infrasound are evident from the direction of the pile fire for filter bands between 2 and 20 Hz (at array FA) and between 5 and 15 Hz (at array FB).

3.2. Video processing

Flame height and flame width evolution are extracted from video (Fig. 3a and 5a) along with spectral information about flame brightness oscillations, or flickering (Fig. 5b). This spectral information comes from pixel brightness variations for the region occupied by the bonfire and follows a technique outlined in [23] where each pixel of the video imagery is treated as its own time series. Pixel brightness values are converted to grayscale and filtered above 1 Hz (with a two pole filter). Those brightness time series with relatively high standard deviations (>1

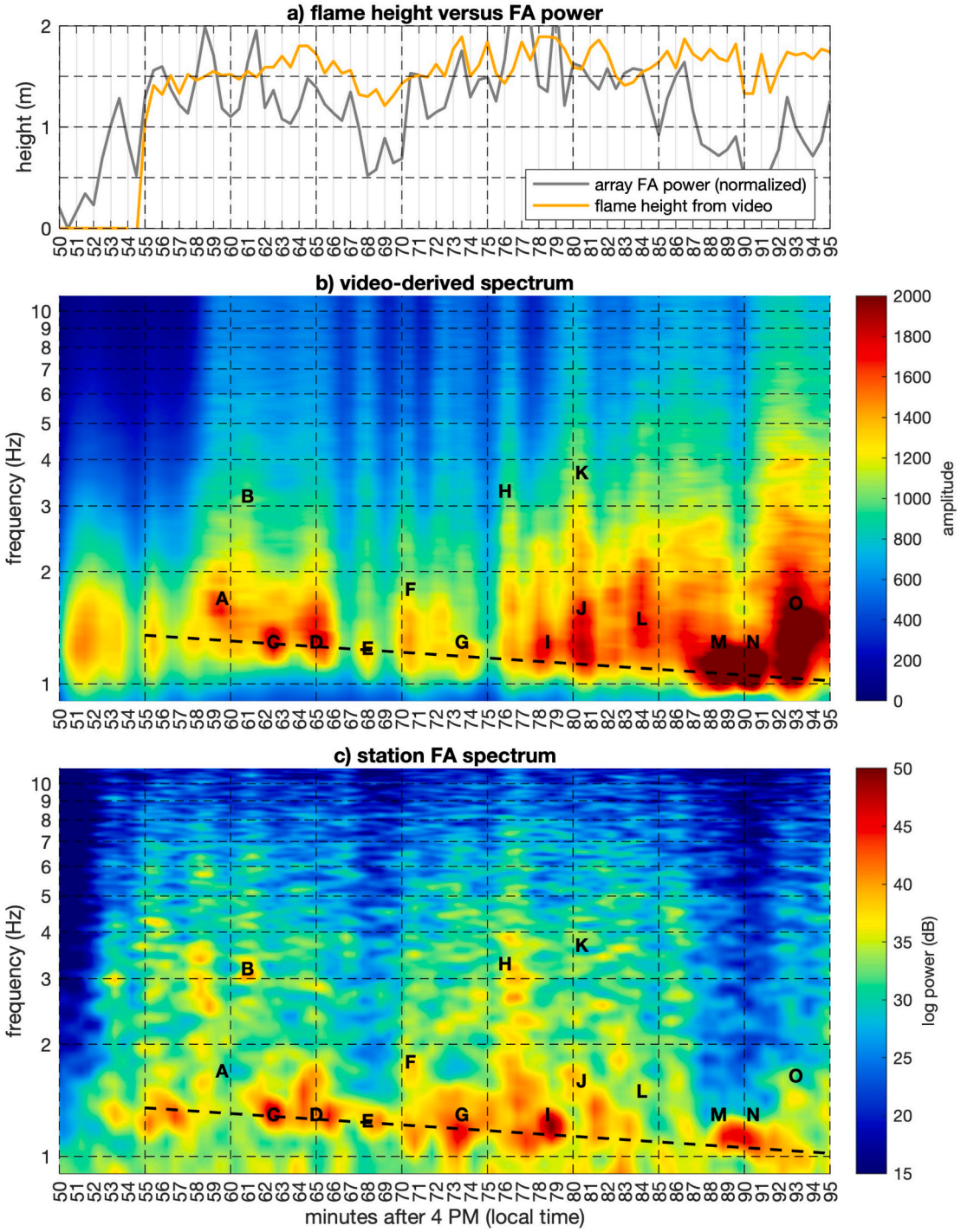

Fig. 5. Comparison of video-derived height and spectra with infrasound-derived power and spectra. (a) Detail of flame height time series and FA power from Fig. 3a and b. (b) Fire spectral information is extracted from video image processsing as described in text. (c) Spectrogram detail is from a zoomed-in portion of Fig. 3c. Letter annotations call attention to certain spectral features, which are common to both video-derived and infrasound-derived spectrograms.

count) are then converted to power spectra and averaged with spectra from other pixels in the video. Because the video sample rate is 25 fps, spectral information extends only up to a 12.5 Hz Nyquist frequency. As with other data analysis, the video spectrogram is calculated using 30 s windows such that it is directly comparable to infrasound data (e.g. Fig. 5c).

4. Results and discussion

The spectral content of the fire infrasound detected for more than one hour at both arrays is better quantified by the signals recorded at FA where fire infrasound pressure is greater and signal to noise is higher (e.g., Fig. 2). At FA a clear division between microbarom infrasound and fire-sourced infrasound is apparent, separated by a spectral trough at about 1 Hz (Figs. 3c and 5c). Above this trough the infrasound power spectra has peaks at about 1.3 Hz at ~5 PM changing toward 1.0 Hz at ~6 PM.

Fluctuations in the recorded video of the pile fire correspond primarily to flame flicker. The spectral manifestation of the video brightness changes is characterized by distinct, short-lived spectral peaks also ranging from 1.3 Hz to 1.0 Hz. This observation points empirically to a common source process for the infrasound that is apparent in video. In particular, some of the same spectral peaks appear coincident for both the infrasound and video-derived spectra occurring at points C, D, E, G, I, M, and N in Fig. 5b and c. We propose that flame flicker is associated with episodic gas pulsing updrafts, which can erupt periodically from the pile fire [24]. This rising gas accelerates the atmosphere, generating infrasound from an effective lumped compact source with frequency content matching the gas pulsing.

Characteristic frequencies in fire infrasound spectra have been previously attributed to puffing during removal of heated boundary layers [15]. The hypothesis is that inflow of air occurs along the base of a pile fire and periodically rises with a frequency ($\boldsymbol{f}$) that relates to square root of the burn diameter ($\boldsymbol{D}$). An empirical relationship of $\boldsymbol{f} = 1.5\boldsymbol{D}^{-0.5}$ was proposed by [12] and matches very well with our frequency observations; infrasonic frequencies transitioning from 1.3 to 1.0 Hz would imply a pile burn diameter changing from 1.3 m to 2.3 m, consistent with our fire dimension (Fig. 3b). That the lowest mode frequency content appears to glide from 1.3 Hz to 1 Hz over the course of an hour may relate to the bonfire becoming wider and/or burning down and becoming less vigorous. Over an hour-long period of time the burn evolved from a flame sourced within the upper portion of the timber pyramid (1–2 m diameter) to a wider burn pile with hot coals spread over a 2–3 m diameter.

Our data also hint at a relationship between fire intensity (quantified by flame height) and infrasound power. In particular, a temporary deficit of infrasound power at array FA between minutes 67 and 70 is correlated with relatively diminished flame activity (Fig. 5a). After minute 120 infrasound radiation at FA drops off significantly as the fire intensity ebbs (Fig. 3a and b). A characteristic unique to burning solids, such as in a pile fire, is the slowing of the combustible mass flux (conversion from solid to gas) over time. This process is driven by ventilation and the changing characteristics of the available remaining hydrocarbons in the solid. A slower/lower mass flux results in a shorter flame, decreasing the heat release rate magnitude, and altering variability of the heat release rate. This reduction in heat release reduces the magnitude of buoyancy driven flow. All of these factors point to a gradually quieter fire in which small changes in mass and heat flux within the contracting flame envelope are likely driving sound generation.

5. Conclusions

Our pile fire recordings extend from an approximate 1.0 to 1.3 Hz mode puffing frequency up into the low frequency audible band. That near-infrasound (1–20 Hz) energy from a pile fire appears to be particularly intense, suggests that distant recordings of fires may be feasible using infrasound, which propagates long distances with relatively low intrinsic attenuation. Although the 1–5 Hz band infrasound was obscured at FB, the 5–15 Hz infrasound at 600 m is detectable for more than one hour despite the fire's small size. We speculate that a larger fire would produce more intense infrasound that should be detectable at further offsets.

Our pile fire was small, but it was an efficient radiator of infrasound in part due to its compact nature; the quarter wavelength of atmospheric sound at 1.0–1.3 Hz is more than 60 m and far larger than the fire's source dimension. A compact source may not be appropriate for a larger wildfire, however, which could extend tens to thousands of meters, and contain a superposition of contributing infrasound sources. Such horizontally extensive source regions may likely radiate infrasound that has a non-symmetric radiation and complex interference pattern. In the case of larger wildfires, deployment of infrasound arrays at a greater distance, where a single lumped backazimuth is identifiable, might be preferable. At the same time, more remote detection of wildfires will have to consider the impact of atmospheric properties, which can refract sound upward during normal stratification or downward during an inversion. In our experiment we have assumed that the effects of a 600-m propagation path are minimal, however future studies will benefit from monitoring of wildfires, small and large, at a range of propagation distances. Given the detectability of a small pile fire at 600 m, we are optimistic that larger fires could be monitored at farther offsets and from locations where safety of field personnel is assured. The promising preliminary results of fire detection with infrasound and infrasound's general utility as a monitoring tool for other hazards suggests that surveillance of wildland fires could benefit firefighting operations by giving early warnings and locations of dangerous changes in fire activity [25]. We propose that further field experimentation is warranted, involving the recording of natural burns or larger prescribed burns at a range of distances. This step will permit a more effective evaluation of infrasound as a remote monitoring tool for fires.

Plain language summary

Wildfires are becoming increasingly common and severe as global warming impacts the environment. As such, there is impetus to develop new technologies to remotely sense and quantify wildfires. Detection and monitoring of wildfires using sub-audible sounds, or infrasound, is one such emerging technology worthy of exploration. Toward the goal of remotely detecting fire with infrasound we conducted a controlled burn experiment with a small pile fire (or bonfire). We recorded its activity with cameras and with infrasound technology using sensors deployed both at near distances (50 m from the fire) and at 600 m from the fire. Using the high signal-to-noise recordings from the closer station we discovered that the dominant sound was inaudible in the infrasound band. This fire infrasound was peaked between 1 and 1.3 Hz and was associated with the pulsing flames of the bonfire. We also demonstrated the capabilities of infrasound monitoring at 600 m to detect the small bonfire. This remote surveillance result is encouraging because we anticipate that larger, more vigorous fires will be detectable at much farther distances permitting infrasound to be developed as an effective ground-based remote sensing tool.

CRediT authorship contribution statement

J.B. Johnson: Writing – review & editing, Writing – original draft, Visualization, Resources, Methodology, Formal analysis, Data curation, Conceptualization. **J.F. Anderson:** Writing – review & editing, Writing – original draft, Visualization, Methodology, Conceptualization. **K. Yedinak:** Writing – review & editing, Formal analysis.

Declaration of competing interest

The authors declare that they have no known competing financial interests or personal relationships that could have appeared to influence the work reported in this paper.

Acknowledgments

Appreciation is extended to M. Hunt, J. Mock, O. Walsh, and C. Johnson for assistance with data collection. This work was supported using overhead return funding from Boise State University.

Data availability

A database with featured video and the infrasonic signals is provided at BSU ScholarWorks in the infrasound data repository with dedicated DOI: https://doi.org/10.18122/infrasound_data.15.boisestate.

References

[1] Watson LM, Iezzi AM, Toney L, Maher SP, Fee D, McKee K, et al. Volcano infrasound: progress and future directions. Bull Volcanol 2022;84(5):44. https://doi.org/10.1007/s00445-022-01544-w.
[2] Che I-Y, Kim K, Le Pichon A, Park J, Arrowsmith S, Stump B. Illuminating the North Korean nuclear explosion test in 2017 using remote infrasound observations. Geophys J Int 2021;228(1):308–15. https://doi.org/10.1093/gji/ggab338.
[3] Johnson JB, Roca A, Pineda A, Mérida R, Escobar-Wolf R, Anderson JF, et al. Infrasound detection of approaching lahars. Sci Rep 2023;13(1):6476. https://doi.org/10.1038/s41598-023-32109-2.
[4] Olivieri M, Piccinini D, Saccorotti G, Barghini D, Gardiol D, Pino NA, et al. The optical, seismic, and infrasound signature of the March 5 2022, bolide over Central Italy. Sci Rep 2023;13(1):21135. https://doi.org/10.1038/s41598-023-48396-8.
[5] Scamfer LT, Anderson JF. Exploring background noise with a large-N infrasound array: waterfalls, thunderstorms, and earthquakes. Geophys Res Lett 2023;50(24). https://doi.org/10.1029/2023GL104635.
[6] White BC, Elbing BR, Faruque IA. Infrasound measurement system for real-time in situ tornado measurements. Atmos Meas Tech 2022;15(9):2923–38. https://doi.org/10.5194/amt-15-2923-2022.
[7] Mutschlecner JP, Whitaker RW. Infrasound from earthquakes. J Geophys Res Atmos 2005;110(D1). https://doi.org/10.1029/2004JD005067.
[8] Anderson JF, Johnson JB, Steele AL, Ruiz MC, Brand BD. Diverse eruptive activity revealed by acoustic and electromagnetic observations of the 14 July 2013 intense vulcanian eruption of tungurahua volcano. Ecuador Geophys Res Lett 2018;45(7):2976–85. https://doi.org/10.1002/2017GL076419.
[9] Arrowsmith SJ, Whitaker R, Taylor SR, Burlacu R, Stump B, Hedlin M, et al. Regional monitoring of infrasound events using multiple arrays: application to Utah and Washington State. Geophys J Int 2008;175(1):291–300. https://doi.org/10.1111/j.1365-246X.2008.03912.x.
[10] Marchetti E, Johnson JB. Infrasound array analysis of rapid mass movements in mountain regions. In: Schmelzbach C, editor. Advances in Geophysics: Geohazards (Advances i, Vol. 64). Zurich: Academic Press; 2023.
[11] Wasserman TN, Mueller SE. Climate influences on future fire severity: a synthesis of climate-fire interactions and impacts on fire regimes, high-severity fire, and forests in the western United States. Fire Ecol 2023;19(1):43. https://doi.org/10.1186/s42408-023-00200-8.
[12] Bedard AJ, Nishiyama RT. Infrasound generation by large fires: experimental results and a review of an analytical model predicting dominant frequencies. In: IEEE International Geoscience and Remote Sensing Symposium. IEEE; 2002. p. 876–8. https://doi.org/10.1109/IGARSS.2002.1025715.
[13] Marcillo O, Yedinak K, Lees JM, Bourne K, Potter B. Seismo-acoustic observations of a prescribed burn. AFE International Fire Ecology and Management Congress, December 2023, Monterey, CA. Oral presentation. 2023.
[14] Anderson JF, Hunt MA, Yedinak KM, Johnson Mapping infrasound emissions for tracking fire activity JB. AFE International Fire Ecology and Management Congress. Monterey, CA: Poster; 2023.
[15] Cetegen BM, Ahmed TA. Experiments on the periodic instability of buoyant plumes and pool fires. Combust Flame 1993;93(1–2):157–84. https://doi.org/10.1016/0010-2180(93)90090-P.
[16] Fang J, Jiang C, Wang J, Guan J, Zhang Y, Wang J. Oscillation frequency of buoyant diffusion flame in cross-wind. Fuel 2016;184:856–63. https://doi.org/10.1016/j.fuel.2016.07.084.
[17] Ihme M, Pitsch H. On the generation of direct combustion noise in turbulent non-premixed flames. Int J Aeroacoust 2012;11(1):25–78. https://doi.org/10.1260/1475-472X.11.1.25.
[18] Yedinak KM, Anderson MJ, Apostol KG, Smith AMS. Vegetation effects on impulsive events in the acoustic signature of fires. J Acoust Soc Am 2017;141(1):557–62. https://doi.org/10.1121/1.4974199.
[19] Marcillo O, Johnson JB, Hart D. Implementation, characterization, and evaluation of an inexpensive low-power low-noise infrasound sensor based on a micromachined differential pressure transducer and a mechanical filter. J Atmos Oceanic Tech 2012;29(9):1275–84. https://doi.org/10.1175/JTECH-D-11-00101.1.
[20] Slad G, Merchant B. Evaluation of low cost infrasound sensor packages. Albuquerque, NM, and Livermore, CA (United States); 2021. doi: 10.2172/1829264.
[21] Bowman JR, Baker GE, Bahavar M. Ambient infrasound noise. Geophys Res Lett 2005;32(9):L09803. https://doi.org/10.1029/2005gl022486.
[22] Neidell N, Taner MT. Semblance and other coherence measures for multichannel data. Geophysics 1971;36(3):482–97. https://doi.org/10.1190/1.1440186.
[23] Johnson JB, Boyer T, Watson LM, Anderson JF. Volcano opto-acoustics: mapping the infrasound wavefield at Yasur Volcano (Vanuatu). Geophys Res Lett 2023. https://doi.org/10.1029/2022GL102029.
[24] Dowling AP, Mahmoudi Y. Combustion noise. Proc Combust Inst 2015;35(1):65–100. https://doi.org/10.1016/j.proci.2014.08.016.
[25] Tedim F, Leone V, Amraoui M, Bouillon C, Coughlan M, Delogu G, et al. Defining extreme wildfire events: difficulties, challenges, and impacts. Fire 2018;1(1):9. https://doi.org/10.3390/fire1010009.